Shot-noise influence on the reconstructed phase image signal-to-noise ratio in digital holographic microscopy

Florian Charrière, Tristan Colomb, Frédéric Montfort, Etienne Cuche, Pierre Marquet, and Christian Depeursinge

In digital holographic microscopy, shot noise is an intrinsic part of the recording process with the digital camera. We present a study based on simulations and real measurements describing the shot-noise influence in the quality of the reconstructed phase images. Different configurations of the reference wave and the object wave intensities will be discussed, illustrating the detection limit and the coherent amplification of the object wave. The signal-to-noise ratio (SNR) calculation of the reconstructed phase images based on the decision statistical theory is derived from a model for image quality estimation proposed by Wagner and Brown [Phys. Med. Biol. **30**, 489 (1985)]. It will be shown that a phase image with a SNR above 10 can be obtained with a mean intensity lower than 10 photons per pixel and per hologram coming from the observed object. Experimental measurements on a glass–chrome probe will be presented to illustrate the main results of the simulations. © 2006 Optical Society of America

OCIS codes: 090.0090, 030.4280, 030.5290, 110.3000.

1. Introduction

Digital holographic microscopy (DHM) is currently undergoing important developments, causing its popularity to increase continually. Its success is due to its capacity to extract both the amplitude and the phase signal of the wavefront diffracted by an object from a hologram recorded through a digital camera and to provide three-dimensional (3D) quantitative phase images. The principle of digital holography (DH) was first proposed by Goodman and Lawrence[1] and by Kronrod *et al*. 30 years ago.[2] At the beginning, holograms were registered on photographic plates, but the digital camera quickly became a more convenient tool. In DH, the intensity distribution of the hologram is processed by a digitally computed replica of the reference wave, after which the amplitude and phase distributions of the complex object wavefront are extracted simultaneously. Quantitative phase information on the nanometer scale is easily achievable with DH and can be extracted from a single hologram.[3,4] The transverse resolution is diffraction limited, as with classical microscopes, but axial resolutions of half a degree have already been reached in a reflection geometry with the phase information DH provides. This corresponds to an axial resolution of approximately 1 nm with a wavelength of 633 nm. Numerous applications and developments based on DH are now being developed. Among others, we can mention DH applications in metrology,[5,6] live cell imaging,[7,8] tomography of biological specimens,[9,10] polarization and birefringence imaging,[11,12] and aberration compensation.[13–15]

Despite the large number of applications and reconstruction methods, to the best of our knowledge, no systematic theory has been developed to quantify the quality of the reconstructed phase images. The most general statistical approach was conducted by Goodman,[16] but most developments were derived in the field of speckle interferometry and are not immediately applicable to the case of specimens with minimum roughness that are mostly investigated in DHM (polished surfaces, clean biological preparations, and optical devices). Some studies on the noise reduction were proposed for specific applications: Monnom *et al*.[17] have demonstrated improved visibility of the reconstructed intensity images by reducing the noise due to out-of-focus objects, but the amelio-

F. Charrière (florian.charriere@a3.epfl.ch), T. Colomb, and C. Depeursinge are with the Imaging and Applied Optics Institute, Ecole Polytechnique Fédérale de Lausanne, CH-1015 Lausanne, Switzerland. F. Montfort and E. Cuche are with the Lyncée Tec SA, PSE-A, CH-1015 Lausanne, Switzerland. P. Marquet is with the Département de Psychiatrie DP-CHUV, Centre de Neurosciences Psychiatriques, Site de Cery, CH-1008 Prilly-Lausanne, Switzerland.

ration is not clearly quantified and the phase behavior is not considered; Paganin et al.[18] investigated the effect of uniformly distributed noise during the acquisition of the out-of-focus images required for their amplitude-based phase-retrieving algorithm, the results being applicable only in their phase-sensitive technique; De Ruijter and Weiss[19] have discussed extensively the detection limit in quantitative off-axis electron holography, but their estimation of the phase variance relies principally on the fringe visibility over the hologram zone from which the phase is deduced, and this estimation therefore only holds with smooth phase variation. We propose here a general model for image quality estimation based on the decision statistical theory proposed by Wagner and Brown.[20] This model is then applied in a study of the influence of shot noise on the reconstructed phase images based on simulations. We will establish the influence of the repartition of the total intensity between the reference and the object beams and the influence of the reference beam intensity for a given object beam intensity. Experimental confirmation of the first simulation will be given.

2. Theory

A. Simulations

Simulated holograms have been used to investigate the behavior of the reconstructed phase images' signal-to-noise ratios (SNRs). The main test object used for simulations is a virtual object representing a mouse neuronal cell, the shape of which has been derived from an actual neuron imaged with DHM presented in Fig. 1(a) (more details on DHM applied to cell imaging can be found in Ref. 8). This test object has been chosen to ensure a broad distribution of spatial frequencies representative of a common imaged object. It is considered a pure phase object (i.e., no absorption) imaged in transmission, for which the measured signal represents the phase shift induced by the specimen, which is proportional to the optical path length resulting from the integration of the refractive index of the specimen along the optical axis. The characteristics of this virtual object imaged in transmission with a $63\times$ microscope objective at a wavelength of $\lambda = 633$ nm are presented in Figs. 1(b) and 1(c). The shape was schematized in order to suppress the noise due to the preparation containing the neuron, but the broad distribution of spatial frequencies was preserved.

The holograms are computed following the off-axis geometry presented in Fig. 1(d). The complex wavefront, resulting from the interaction of the illumination plane wave with our pure phase object, is propagated along a distance $d = 20$ cm according to the Fresnel approximation, to figure the acquisition of a nonfocused complex field on the CCD camera. The number of pixels considered for the object wavefront and for the hologram is $N = 512 \times 512$. The size of the hologram and of the virtual object is 5.12 mm $\times$ 5.12 mm, corresponding to the size of the real image of a mouse neuron cell seen through a microscope
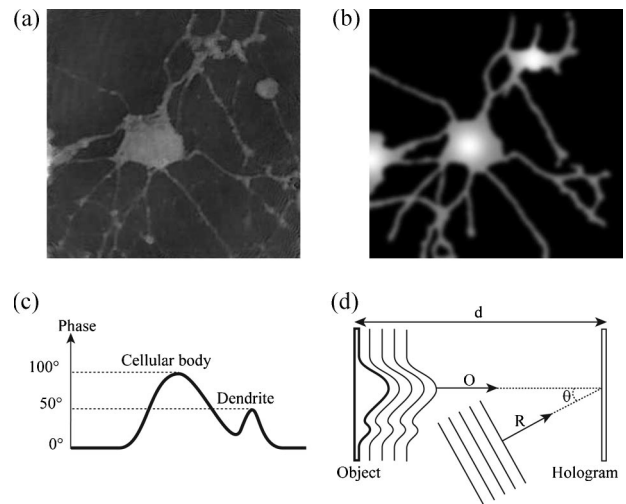

Fig. 1. (a) Real neuron phase image registered with DHM, (b) virtual neuron phase image, (c) virtual neuron characteristics summary, and (c) schematic of the off-axis hologram simulation (propagation of the wavefront on a distance d via the Fresnel integral): O, object wave; R, reference wave.

objective ($63\times$ magnification).[8] The off-axis hologram is obtained by computing the interference between the propagated object wave and a plane reference wave, whose propagation direction defines an angle $\theta = 0.7°$ with respect to the object wave propagation direction. Then shot noise is introduced on the image to simulate a real recorded intensity. The shot noise follows a Poisson's statistic[6]; i.e., the variance of the number of photons hitting a single pixel of the detector equals the mean number of photons hitting this pixel. The image is stored in an 8-bit image format, considering an ideal detector, which can set the lower intensity value to 0 and the maximum value to 255.

B. Processing the Hologram by the Convolution Approach

The method used to process the simulated holograms is based on the convolution approach described by Schnars and Jüptner in Ref. 4. The main advantage of this method is that the pixel sizes of the image and of the hologram are equal. It is therefore convenient to compute the SNR with the formula of Eq. (1) because the correspondence between a reconstructed image point and the initial object point is straightforward. With the other classical Fresnel–Kirchhoff integral reconstruction, described in Refs. 3 and 4, a rescaling of the reconstructed image is necessary for a pixel-to-pixel comparison, which can introduce some additional numerical noise. As described in Ref. 21, the removal of the zero order and of the twin image as well as the spatial filtering is performed by applying a user-defined mask to the Fourier spectrum of the off-axis hologram.

The intensity distribution in the hologram plane can be described by the following expression:

$$I_H(x,\ y) = \underbrace{OO^* + RR^*}_{\text{zero order}} + \underbrace{OR^*}_{\text{real image}} + \underbrace{R^*O}_{\text{virtual image}},\quad (1)$$

where O and R are, respectively, the interfering object and reference. In classical holography, the reconstruction of the wavefront is achieved by illuminating the hologram with a replica of the reference wave. The wavefront $\Psi(x, y) = \mathbf{R}(x, y)I_H(x, y)$ propagates toward an observer, where the 3D image of the object is reconstructed. In digital holography, the reconstruction of the wavefront $\Psi(k\bar{x}, l\bar{y})$, where $\bar{x}$ and $\bar{y}$ are the pixel size of the CCD and k and l are integer values, is obtained the same way by multiplying the hologram intensity distribution $I_H(k, l)$ with a digitally computed reference wave $\mathbf{R}_D(k, l)$, called the digital reference wave. Assuming a plane reference wave, $\mathbf{R}_D$ can be described as follows:

$$\mathbf{R}_D(k, l) = A_R \exp[i(k_{Dx}k\bar{x} + k_{Dy}l\bar{y})], \qquad (2)$$

where k_{Dx} and k_{Dy} are the two components of the wave vector in the hologram plane and A_R is an amplitude constant. The digitally reconstructed wavefront $\Psi(k\bar{x}, l\bar{y})$ is first computed in the hologram plane $x_0 y_0$ and can afterward be evaluated at any distance from the hologram plane by the calculation of the scalar diffraction of the wavefront in the Fresnel approximation. $\Psi(m\Delta\xi, n\Delta\eta)$ is computed at a distance d from the hologram plane, in an observation plane $O\xi\eta$, by use of the following Fresnel propagation formula:

$$\Psi(m\Delta\xi, n\Delta\eta) = A\Phi(m, n)\mathrm{FFT}^{-1}\{\mathrm{FFT}[\mathbf{R}_D(k, l) \\ \times I_H(k, l)]_{p,q}\exp[-i\pi\lambda d(p^2 + q^2)]\}_{m,n}, \qquad (3)$$

where p, q and m, n are integers ($-N/2 \le m$, $n < N/2$), FFT is the fast Fourier transform operator, FFT^{-1} is the inverse fast Fourier transform operator, $A = \exp(i2\pi d/\lambda)/(i\lambda d)$ is a propagation constant, and $\Phi(m, n) = \exp[-i\pi/(\lambda d_1)m^2\Delta\xi^2 - i\pi/(\lambda d_2)n\Delta\eta^2]$ is the so-called digital phase mask with parameters d_1 and d_2 digitally adjusted to correct the phase aberration due to the microscope objective. $\Delta\xi = \bar{x}$ and $\Delta\eta = \bar{y}$ are the sampling intervals in the observation plane.

Considering only the virtual images of Eq. (1), the propagated wavefront corresponding to the computed digital reference wave is

$$\Psi = \mathbf{R}_D\mathbf{R} * \mathbf{O}, \text{ with } \mathbf{R}_D = \exp[i(k_{Dx}k\bar{x} + k_{Dy}l\bar{y})], \qquad (4)$$

where k_{Dx} and k_{Dy} are two parameters adjusted to achieve identical propagation directions for $\mathbf{R}$ and $\mathbf{R}_D$.

Equation (3) requires the adjustment of four parameters for the proper reconstruction of the phase distribution. k_{Dx} and k_{Dy} compensate for the tilt aberration resulting from the off-axis geometry or resulting from an imperfect orientation of the specimen surface, which should be accurately oriented perpendicular to the optical axis. d_1 and d_2 correct the wavefront curvature induced by the microscope objective according to a parabolic model. Note that in the present study, these last two parameters only need to be adjusted during the processing of real acquired holograms because in the simulation no curvature induced by the microscope objective was considered. As explained in Ref. 3, the parameter values are adjusted in order to obtain a constant and homogeneous phase distribution on a flat reference surface located in or in the proximity of the specimen. The manual procedure described in Ref. 3 has been implemented here as a semiautomated procedure. First, the program extracts two lines—a horizontal line along 0ξ and a vertical line along 0η—whose location is defined by the operator in the reference surface. Then 1D phase data extracted along the two lines are unwrapped[22] to remove 2π phase jumps, and a curve-fitting procedure is applied to evaluate the unwrapped phase data with a 1D polynomial function of the second order. k_{Dx} and d_1 are iteratively adjusted to minimize the deviation between the fitted curve and the ideal horizontal constant profile. Similarly, k_{Dy} and d_2 are adjusted until the vertical profile is as close as possible to the ideal vertical constant profile. In general, less than five iterations are necessary to reach optimal parameter values. If a reference area is not available on the specimen, the parameters are first calculated on another reference surface (air in transmission, a mirror in reflection); then a simple digital tilt adjustment of the phase, corresponding to an adjustment of k_{Dx} and k_{Dy}, is performed with the same procedure described above when the specimen is observed.

Note that this digital adjustment method has been generalized to a multiprofile automatic procedure with a correction of the optical aberrations of the higher order. An extensive description of the technique and its applications to specimen shape compensation is presented in Ref. 15.

C. Signal-to-Noise Ratio of Phase Images

The SNR evaluation of an arbitrary image based on the statistical decision theory, proposed by Wagner and Brown,[20] is calculated according to the following expression:

$$\mathrm{SNR} = \frac{\int\int \mathrm{d}f_x\mathrm{d}f_y|F[S(x, y)]|^2}{\sqrt{\int\int \mathrm{d}f_x\mathrm{d}f_y|F[S(x, y)]|^2 \, W(f_x, f_y)}}, \qquad (5)$$

where $S(x, y)$ is the signal describing our image, F is the Fourier transform, and $W(f_x, f_y)$ is the Wiener spectrum of the noise, expressed by

$$W(f_x, f_y) = \lim_{L_x, L_y \to \infty} \frac{1}{4L_xL_y}\left|\int_{-L_x}^{L_x}\mathrm{d}x\int_{-L_y}^{L_y}\mathrm{d}y\Delta S(x, y)\right. \\ \left.\times \exp[-2\pi i(xf_x + yf_y)]\right|^2, \qquad (6)$$

where $\Delta S(x, y)$ is the absolute variation of $S(x, y)$ caused by the noise. This SNR provides an absolute scale for image system performance assessment and leads to instrumentation design goals and constraints for imaging system optimization since no observer can surpass the performance of the ideal observer. The dependence of the detectable detail size on exposure or imaging time follows immediately from the analysis (see Ref. 20 for details). This expression assumes the case of a quasi-ideal observer needing to determine whether a well-known specific object described by the function $S(x, y)$ is present in the field of view: The higher the SNR, the higher the object presence probability. A white noise is considered, even if the image noise is colored. An extention of this theory to a perfect observer who does not have this limitation is possible, and, in this case, the SNR expression presented here corresponds to the lower bound of the extended SNR, i.e., the most pessimistic SNR value.

Complete *a priori* knowledge of $S(x, y)$ is necessary to measure the SNR with this expression to allow a proper computation of the Wiener spectrum. This can easily be performed with simulations, because the image object is perfectly known, but can become difficult in real measurements.

D.   Signal-to-Noise Ratio of the Hologram

To give a more intuitive description of the behavior of the phase image SNR in some particular limit cases described in Section 3, it is useful also to evaluate the SNR of the hologram itself. When two waves interfere, in our case, an object wave with intensity I_{Obj} and a reference wave with intensity I_{Ref}, the intensity of the interference pattern may be expressed as

$$I_{\text{interference}} = I_{\text{Obj}} + I_{\text{Ref}} + \sqrt{I_{\text{Obj}} I_{\text{Ref}}} \cos(\varphi), \qquad (7)$$

where φ is the phase difference between the two waves. The maximal variation of the amplitude is $2\sqrt{I_{\text{Obj}} I_{\text{Ref}}}$, as $\cos(\varphi)$ can take values between -1 and 1. In our study, the 8-bit detector is assumed to be perfect; i.e., the minimal intensity is set to 0 and the maximal intensity is set to 255. The maximal signal therefore corresponds exactly to the amplitude variation of $2\sqrt{I_{\text{Obj}} I_{\text{Ref}}}$. For a given pixel on the hologram, the maximal SNR value on the hologram can be expressed as

$$\text{SNR}_{\text{holo}} = \frac{2\sqrt{I_{\text{Obj}} I_{\text{Ref}}}}{\sqrt{I_{\text{Obj}} + I_{\text{Ref}}}}, \qquad (8)$$

where the numerator is the maximal signal collected on a given pixel, and the denominator is the corresponding shot noise.

3.   Results and Discussion

In what follows, the so-called total intensity represents the mean intensity diffracted by the object I_{Obj} added to the reference wave intensity I_{Ref}. For the simulations, the ideal function $S(x, y)$ corresponds to
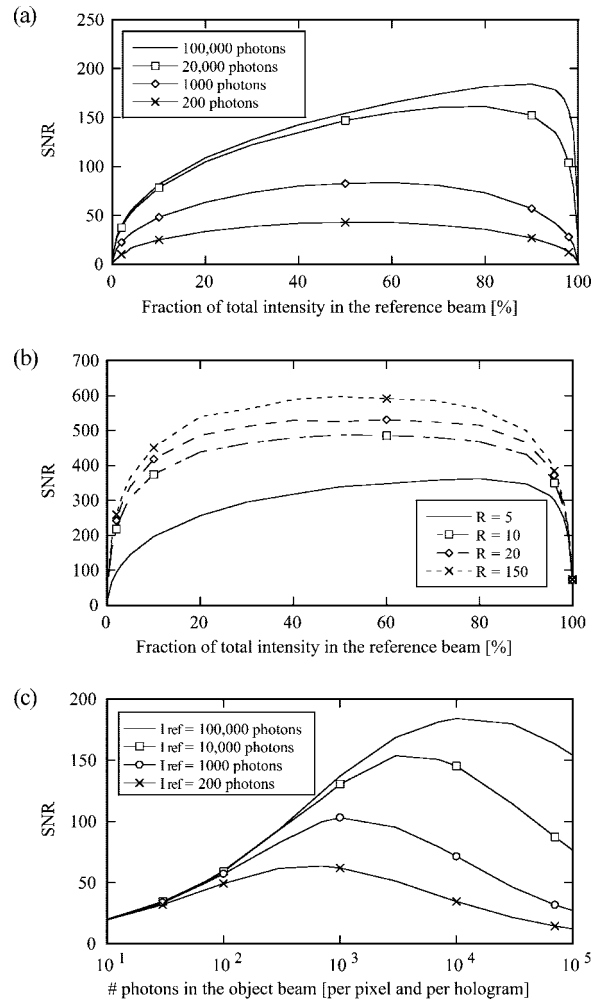

Fig. 2.   (a) SNR on the neuron phase image as a function of the repartition of the total intensity between the two beams for different total intensities, (b) SNR on Gaussian objects as a function of the repartition of the total intensity between the two beams for a different object radius, and (c) SNR on the neuron phase image as a function of the object intensity for different reference intensities.

the phase function of the virtual neuron [see Fig. 1(c)], while the absolute variation $\Delta S(x, y)$ is calculated as the absolute difference between $S(x, y)$ and the phase of Ψ [Eq. (4)], the actual phase signal reconstructed from the hologram taking the shot noise (Poisson's statistic) into account.

A first simulation shows that, in the case of a constant total intensity, a variation in the repartition of this intensity between the reference and the object beam is followed by a variation of the reconstructed image SNR. Figure 2(a) represents the SNR curves as a function of the percentage of intensity in the plane reference wave; the different curves are obtained for different total intensities expressed in the total number of photons per pixel and per hologram, the values of which are shown on the graphic. It can be observed that the SNR decreases abruptly at both graph extremities, when almost the total intensity is concentrated in either the reference or the object beam, i.e., when one of

the intensities tends to zero. This is easily understood when calculating the limits of Eq. (8):

$$\lim_{I_{\text{Obj}} \to 0} \text{SNR}_{\text{holo}} = \frac{2\sqrt{I_{\text{Obj}}I_{\text{Ref}}}}{\sqrt{I_{\text{Obj}} + I_{\text{Ref}}}} = \frac{0}{\sqrt{I_{\text{Ref}}}} = 0, \qquad (9)$$

$$\lim_{I_{\text{Ref}} \to 0} \text{SNR}_{\text{holo}} = \frac{2\sqrt{I_{\text{Obj}}I_{\text{Ref}}}}{\sqrt{I_{\text{Obj}} + I_{\text{Ref}}}} = \frac{0}{\sqrt{I_{\text{Obj}}}} = 0. \qquad (10)$$

If the SNR of the hologram tends to be zero, it is obvious that the SNR of the reconstructed phase images also becomes zero. In Fig. 2(a), it can be seen that for a low total intensity, the SNR curve is symmetric with respect to the intensity distribution and the maximal SNR value comes for an equal intensity repartition in each beam: At lower intensities, the SNR on the hologram is quite low and its maximum, i.e., the maximum of the expression $2\sqrt{I_{\text{Obj}} I_{\text{Ref}}}$, appears when both intensities are equal. Figure 2(a) also shows that for an intensity close to the camera saturation (camera saturation intensity is commonly around 100,000 photons per pixel for a camera with a gain of 1), the SNR maximum is clearly not centered and one had better put more intensity in the reference beam to increase the SNR. This dissymmetry discovered thanks to the simulation is more difficult to understand intuitively. One interpretation can be the following: The shot-noise perturbation on the hologram for a given pixel depends on the total intensity impinging on this pixel; if the intensity on each pixel comes mainly from the reference beam that is uniform over the hologram, the shot-noise perturbation on the hologram is much more uniform, and therefore uniformly distributed in the spectrum of the hologram, compared to a nonuniform noise distribution following the object beam intensity, and consequently the object spatial frequencies, in the case of a more intense object beam. One must also note that the maximum SNR value not only depends on the total intensity but also depends on the complexity of the object spectrum. To illustrate this fact, holograms were generated with some Gaussian phase objects characterized by a maximal phase value of π and an adjustable width defined by R, the radius in number of pixels taken at the FWHM value of the Gaussian phase object. The curves, calculated for a total average intensity of 100,000 photons per pixel and per hologram, are shown in Fig. 2(b); the different curves correspond to the different values of R chosen. It is clear that the SNR reaches greater values for broader phase objects with a thinner spectrum. For broader phase objects also, the shape of the curve is more symmetric, due to the simpler form of the object and its correspondent thin spectrum: For great values of R, the broad Gaussian phase objects tend to resemble a plane wave, making the system more and more symmetric. The results of these first two simulations should play a role of primary importance in the design of an experimental DHM setup, as one can usually distribute arbitrarily the intensity of the laser
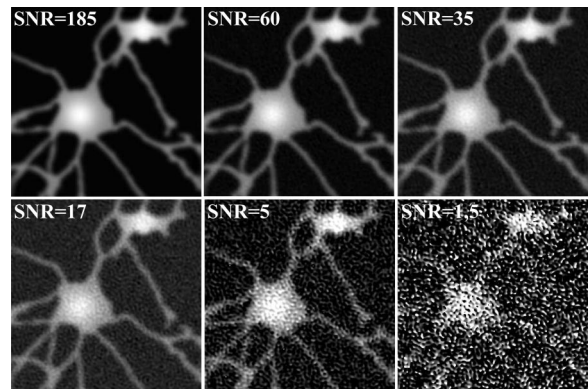

Fig. 3. Degradation of the reconstructed neuron phase image for different SNR values.

source between the reference and the object beam of the interferometer.

A second simulation presented in Fig. 2(c) shows the SNR curves as a function of the intensity in the object beam for a constant reference beam intensity; the different curves are obtained for different reference beam intensities (also in mean number of photons recorded per pixel and per hologram). This graphic illustrates that for a given intensity of the object beam, it is possible to improve the reconstructed image SNR by simply increasing the reference intensity. This gain in SNR is due to the coherent amplification of the object beam by the reference beam during the hologram acquisition. The maximum SNR improvement depends on the intensity coming from the object, and no significant improvement can be observed below a mean number of ten photons per pixel and per hologram. As before, this saturation of the SNR is understood when looking at what happens to the SNR of the hologram:

$$\lim_{I_{\text{Ref}} \to \infty} \text{SNR}_{\text{holo}} = \frac{2\sqrt{I_{\text{Obj}}I_{\text{Ref}}}}{\sqrt{I_{\text{Obj}} + I_{\text{Ref}}}} = \frac{2\sqrt{I_{\text{Ref}}}\sqrt{I_{\text{Obj}}}}{\sqrt{I_{\text{Ref}}}\sqrt{\frac{I_{\text{Obj}}}{I_{\text{Ref}}} + 1}} = 2\sqrt{I_{\text{Obj}}}.$$

$$(11)$$

This limit calculation illustrates that the upper limit of the hologram SNR is determined by the object beam intensity only. It also shows that thanks to the coherent detection, the SNR on the hologram is twice as high as it would be with standard intensity image detection.

The images presented in Fig. 3 show the evolution of the reconstructed phase images for the neuron with a decreasing SNR to illustrate how the degradation of the image occurs.

To illustrate the results obtained with simulations, some measurements on a glass–chrome probe were made with a reflection DHM setup, schematically shown in Fig. 4. The laser source used is a 635 nm laser diode by Coherent, the camera is an 8-bit, black-and-white, 512×512 pixel (9.47 μm size) Hitachi CCD, and the microscope objective has a magnification of 10× and a numerical aperture of 0.30. A
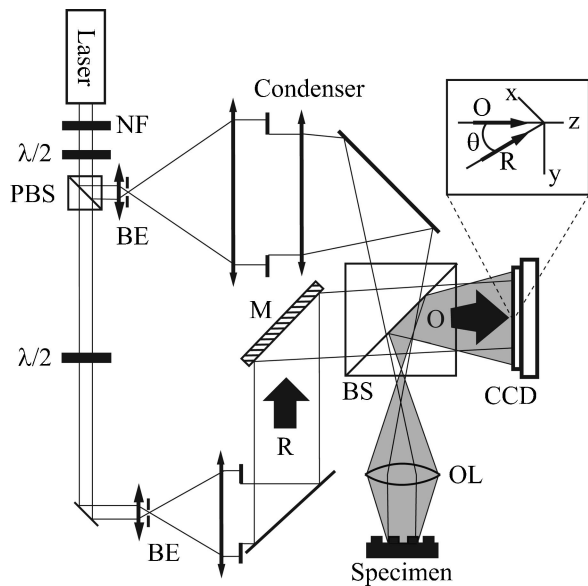
Fig. 4. Schematic of the holographic microscope for reflection imaging. NF, neutral-density filter; PBS, polarizing beam splitter; BE, beam expander with spatial filter; λ/2, half-wave plate; M, mirror; BS, beam splitter; O, object wave; R, reference wave.

quartz–chrome binary grating was used as the test object. Figures 5(a) and 5(b) resume the properties of the specimen. This grating was chosen because its Fourier spectrum is broad enough (high spatial frequencies due to abrupt steps), and its simple precise shape allows us to define an exact mathematical description of the grating to properly calculate the SNR according to Eq. (5), which is much more complicated if not impossible with mouse neurons because their shape is not known *a priori*. Figure 6 resumes the experimental realization of the first simulation, in which the total intensity is constant, here approximately 20,000 photons per pixel and per hologram, but the repartition of the intensity in the two beams varies. Repartition was simply adjusted with the help of the first λ/2 combined with the polarizing beam splitter. The asymmetry in the SNR curve with respect to the intensity repartition observed in the simulation [Fig. 2(a)] is also clearly reproduced in the
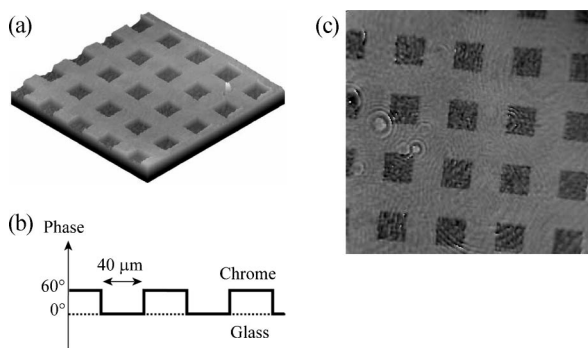

Fig. 5. (a) Glass–chrome specimen reflection DHM phase image perspective, (b) specimen characteristics summary, and (c) specimen phase image for an average illumination intensity of 2.9 nW/cm².
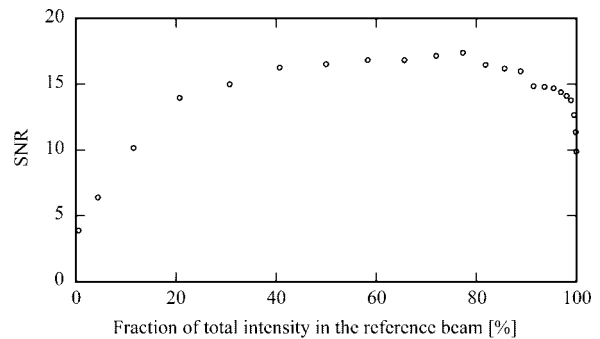

Fig. 6. SNR of the glass–chrome probe phase image as a function of the repartition of the total intensity between the two beams.

experiment, confirming the advantage of putting more intensity in the reference beam as in the object beam to improve the SNR. Just to illustrate that imaging at very low object intensity is possible, as predicted by previous simulations, a phase image of the glass–chrome specimen was taken with a diffracted object intensity of 2.9 nW/cm², corresponding approximately to 170 photons per pixel and per hologram for an integration time of 0.02 s. The SNR of this phase image, shown in Fig. 5(c), is 9.9. Concentric circles and parasitic fringes on the image are due to coherent noise (multiple reflections of the beams on the optics of the setup, especially the microscope objective) and are much more limiting for low object intensity imaging than for shot noise in the presented setup. The important readout noise of the CCD used is also a strong limitation, so that imaging with a few photons per pixel and per hologram becomes really difficult in our case.

Even if the real measurements reproduce the simulation qualitatively well, a note needs to be made about the numerical values reached by the SNR. As already mentioned above, an exact numerical description of the object is required to compute the SNR. The superposition of the numerical description of the object and the reconstructed phase image of the object was done with a maximal precision of one pixel. The present DHM setup is subject to coherent noise due to the large coherence length of the laser source: Interference patterns, which were not considered in simulations, appear on the hologram due to multiple reflections on optical components in the system. Finally, our detector is, of course, not ideal: The dynamic range is manually adjusted, and the readout noise is not negligible. This passage from the simulated world to the real world therefore drastically diminishes the highest values reached by the SNR, but the behavior of the curves is preserved.

4. Conclusion

The SNR model, based on the decision statistical theory, applied here to evaluate the behavior of DHM phase images under the influence of the shot noise, is a general tool for image quality estimation. Even if its application on real phase images may be difficult, owing to the required *a priori* description of the

object, it is readily adapted to studies based on simulations. Evaluations of important DHM processes, involving reconstruction algorithms, filtering techniques, and different noise models, can be envisaged this way.

Results obtained during the present work with simulations on total intensity repartition between the reference beam and the object beam are directly applicable to the experimental setup in order to reduce the shot-noise influence in reconstructed phase images. For the first time, to our knowledge, it has been demonstrated that in some cases a reference beam with its intensity equal to the object beam intensity is not the most favorable case regarding the reconstructed phase image quality. The influence on the phase signal SNR thanks to the object beam coherent amplification in digital holography has also been illustrated for the first time.

References

1. J. W. Goodman and R. W. Lawrence, "Digital image formation from electronically detected holograms," Appl. Phys. Lett. **11**, 77–79 (1967).
2. M. A. Kronrod, N. S. Merzlyakov, and L. P. Yaroslavskii, "Reconstruction of a hologram with a computer," Sov. Phys. Tech. Phys. **17**, 333–334 (1972).
3. E. Cuche, P. Marquet, and C. Depeursinge, "Simultaneous amplitude and quantitative phase-contrast microscopy by numerical reconstruction of Fresnel off-axis holograms," Appl. Opt. **38**, 6994–7001 (1999).
4. U. Schnars and W. P. O. Jüptner, "Digital recording and numerical reconstruction of holograms," Meas. Sci. Technol. **13**, R85–R101 (2002).
5. V. Kebbel, J. Muller, and W. P. O. Jüptner, "Characterization of aspherical micro-optics using digital holography: improvement of accuracy," in *Interferometry XI: Applications,* Proc. SPIE **4778**, 188–197 (2002).
6. F. Charrière, J. Kühn, T. Colomb, F. Montfort, E. Cuche, Y. Emery, K. Weible, P. Marquet, and C. Depeursinge, "Characterization of microlenses by digital holographic microscopy," Appl. Opt. **45**, 829–835 (2006).
7. G. Popescu, L. P. Deflores, J. C. Vaughan, K. Badizadegan, H. Iwai, R. R. Dasari, and M. S. Feld, "Fourier phase microscopy for investigation of biological structures and dynamics," Opt. Lett. **29**, 2503–2505 (2004).
8. P. Marquet, B. Rappaz, P. J. Magistretti, E. Cuche, Y. Emery, T. Colomb, and C. Depeursinge, "Digital holographic microscopy: A noninvasive contrast imaging technique allowing quantitative visualization of living cells with subwavelength axial accuracy," Opt. Lett. **30**, 468–470 (2005).
9. M. K. Kim, "Tomographic three-dimensional imaging of a biological specimen using wavelength-scanning digital interference holography," Opt. Express **7**, 305–310 (2000).
10. F. Charrière, F. Montfort, J. Kühn, T. Colomb, A. Marian, E. Cuche, P. Marquet, and C. Depeursinge, "Cell refractive index tomography by digital holographic microscopy," Opt. Lett. **31**, 178–180 (2006).
11. S. Grilli, P. Ferraro, M. Paturzo, D. Alfieri, and P. De Natale, "*In situ* visualization, monitoring and analysis of electric field domain reversal process in ferroelectric crystals by digital holography," Opt. Express **12**, 1832–1842 (2004).
12. T. Colomb, E. Cuche, F. Montfort, P. Marquet, and C. Depeursinge, "Jones vector imaging by use of digital holography: simulation and experimentation," Opt. Commun. **231**, 137–147 (2004).
13. P. Ferraro, S. De Nicola, A. Finizio, G. Coppola, S. Grilli, C. Magro, and G. Pierattini, "Compensation of the inherent wave front curvature in digital holographic coherent microscopy for quantitative phase-contrast imaging," Appl. Opt. **42**, 1938–1946 (2003).
14. C. Liu, Z. G. Liu, F. Bo, Y. Wang, and J. Q. Zhu, "Digital holographic aberration compensation in electron holography," Opt. Eng. **42**, 651–655 (2003).
15. T. Colomb, E. Cuche, F. Charrière, J. Kühn, N. Aspert, F. Montfort, P. Marquet, and C. Depeursinge, "Automatic procedure for aberrations compensation in digital holographic microscopy and applications to specimen shape compensation," Appl. Opt. **45**, 851–863 (2006).
16. J. W. Goodman, *Statistical Optics* (Wiley, 1985).
17. O. Monnom, F. Dubois, C. Yourassowsky, and J. C. Legros, "Improvement in visibility of an in-focus reconstructed image in digital holography by reduction of the influence of out-of-focus objects," Appl. Opt. **44**, 3827–3832 (2005).
18. D. Paganin, A. Barty, P. J. McMahon, and K. A. Nugent, "Quantitative phase-amplitude microscopy. III. The effects of noise," J. Microsc. **214**, 51–61 (2004).
19. W. J. De Ruijter and J. K. Weiss, "Detection limits in quantitative off-axis electron holography," Ultramicroscopy **50**, 269–283 (1993).
20. R. F. Wagner and D. G. Brown, "Unified SNR analysis of medical imaging-systems," Phys. Med. Biol. **30**, 489–518 (1985).
21. E. Cuche, P. Marquet, and C. Depeursinge, "Spatial filtering for zero-order and twin-image elimination in digital off-axis holography," Appl. Opt. **39**, 4070–4075 (2000).
22. H. Takajo and T. Takahashi, "Noniterative method for obtaining the exact solution for the normal equation in least-squares phase estimation from the phase difference," J. Opt. Soc. Am. A **5**, 1818–1827 (1988).